A Segmentation Strategy for Structures with Common Mode Coupling

James Hunter¹, Shengxuan Xia², Aaron Harmon³, Mohamed Z. M. Hamdalla*⁴, Ahmed M. Hassan*⁵, Victor Khilkevich⁶, Daryl G. Beetner⁷
EMC Laboratory, Missouri University of Science and Technology, Rolla, MO, USA
*University of Missouri Kansas City, Kansas City, MO, USA

¹jdhzg8@mst.edu, ⁷daryl@mst.edu

Abstract— The level of electromagnetic coupling to electronic devices can vary widely from one device to another. When considering the induced voltage from an incoming plane wave on printed circuit boards (PCBs) and their attached cable harnesses, there is significant variety in the configuration of the devices that could be seen. This encourages the use of segmentation, so that the components of these devices (PCBs, connectors, and harnesses) can be modeled separately to alleviate simulation burden. This allows for a more flexible model and a "toolbox" to construct devices with. The goal of this work is to use segmentation to model the external electromagnetic radiation from these devices. The radiation pattern and reciprocity theory can later be used to calculate the voltage coupled from an incident plane wave. Most realistic devices exhibit strong common mode (or antenna mode) coupling that cannot be ignored during segmentation. When segmenting such structures, a multi-modal approach is needed to incorporate coupling from both the common (CM) and differential (DM) modes and to allow these currents to flow properly between the blocks. This work introduces the concept by segmenting a simple dipole, which requires the common mode only, and then applies the complete methodology to a more complicated structure that requires the incorporation of both modes.

Keywords — common mode, differential mode, electromagnetic coupling, harness segmentation.

I. INTRODUCTION AND PROBLEM FORMULATION

The coupling of external radiation to an electronic device can be found through careful testing [1] or through simulations of highly detailed electromagnetic models [2], but at a high computational cost when there is a wide variety of devices that need to be characterized. A modern device typically includes printed circuit boards (PCBs), cables or wire harnesses, and connectors between them. At relatively low frequencies, most energy couples to larger structures such as cables, PCB planes, enclosures, etc. At gigahertz frequencies, smaller structures like PCB traces and integrated circuit (IC) packages become important. Both classes of structures should be accurately modeled to properly estimate the coupling that can be expected when illuminating the device with a signal containing energy from hundreds of megahertz to several gigahertz. However, including objects of vastly different electrical size into one model can lead to a prohibitively long simulation time with excessive memory requirements. To alleviate this problem, a segmentation strategy is applied where certain parts of the structure are simulated separately, and the results are later combined [3-5]. The following paper summarizes work performed to develop a model of coupling to simplified

Supported by the Office of Naval Research (ONR) N00014-17-1-3016 ©2022 IEEE

electronic devices, including harnesses, connectors, and PCB traces.

Previously, two studies were performed to estimate the statistical variations in coupling among a range of characteristics of the device of interest, but this work only investigated coupling to one-wire harnesses [6] and the devices were characterized through bulk simulation [7]. A much more flexible model is needed to characterize a wider range of devices (including different harness configurations, PCB form factors, trace routings, IC package geometries, etc.). Hence, the desire for a segmented model that allows for individual analysis of the PCB, connector, and harness.

First, consider a simple segmentation example of a translationally invariant two-wire transmission line in Fig. 1. Suppose two identical segments are created by cutting the transmission line in the middle. To combine the segments, a port at the segmentation interface should be defined. An important condition for successful segmentation is that the fields at the segmentation port can be represented as a linear combination of the port modes. In other words, that the set of the port modes forms a basis for the field existing in the original structure in the segmentation plane [8-10]. Segmentation is routinely used every time network parameters (such as S-parameters) are defined. Usually, this technique is applied to transmission lines (TL) when the end goal of segmentation is to calculate, for example, the transmission coefficient between the source and load connected to opposite ends of a TL. Then, the choice of the modes in the segmentation port becomes straightforward. A linear combination of the modes capable of propagating in the given TL cross-section gives an exact representation of the field in the original (unsegmented) TL (provided that the segmentation plane is far enough from TL discontinuities and that the amplitudes of the evanescent modes at the segmentation interface are negligible). This type of segmentation calls for the definition of the differential TEM mode at the segmentation interface of the structure in Fig. 1. The electrical field distribution of this mode is show in Fig. 2.

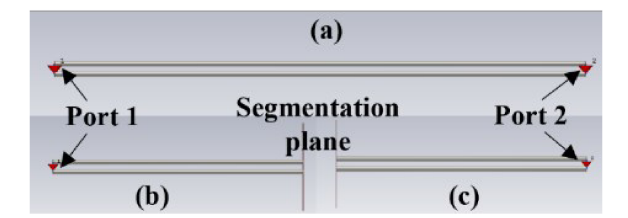


Fig. 1. (a) Two-wire transmission line for segmentation. The line is cut in the middle creating two identical segments: (b) segment 1, (c) segment 2.

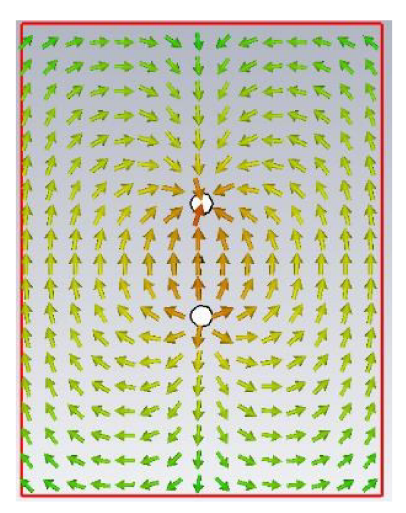


Fig. 2. Electrical field of the differential TEM mode of the two-wire transmission line.

Now, suppose that the two-wire line is illuminated by a plane wave. The plane wave will most likely excite some differential mode in the TL, but additionally the antenna mode, or a common mode, will be excited. This mode forces the current in both conductors to flow in the same direction. This mode could be also called a dipole mode in the sense that the field structure would be similar (if not identical) to the field produced by a dipole (or a linear wire antenna more generally). This mode is shown in Fig. 3a and was obtained by defining a discrete port in series with each conductor of the transmission line and driving the ports in phase in order to impose a current flowing in the same direction on each conductor, Fig. 3b.

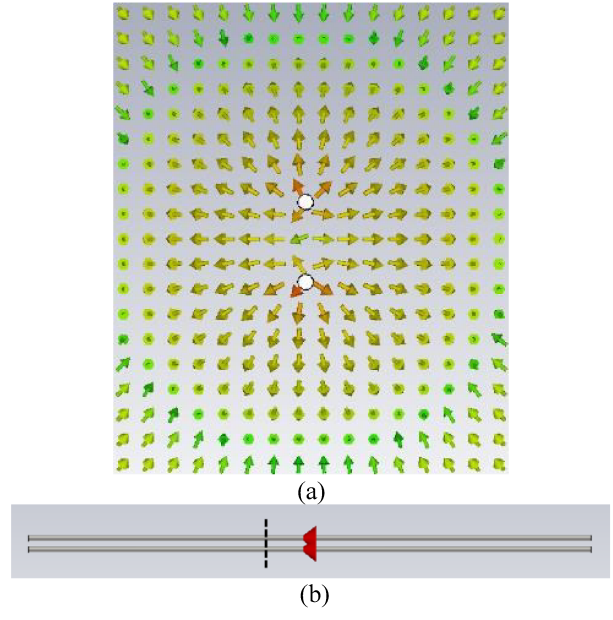


Fig. 3. (a) Electrical field distribution of the common mode of the twowire transmission line. (b) Simulation model used to excite the common mode of the two-wire transmission line by defining discrete ports in

series with the conductors. The vertical dashed line denotes the location of the plane where the field distribution in (a) was measured.

The mode in Fig. 3 is different from traditional port modes in one important aspect: the energy in that mode would be transferred not only through the segmentation plane (i.e., parallel to the TL), but also parallel to the segmentation plane (i.e., perpendicular to the TL) due to radiation from the dipole. At the same time, the field distribution (at least close to the conductors) resembles that of the TEM mode propagating along the conductors, which suggests that the TEM mode could be used at least as an approximation of the CM field and facilitate the segmentation of structures with significant common mode coupling.

The scope of this paper is therefore investigation of the possibility to segment realistic structures with significant coupling from the CM and a technical implementation of the approach using CST Microwave Studio software.

II. DIPOLE SEGMENTATION WITH COMMON MODE

As a first example, consider a simple dipole 60 cm in total length, which is symmetrical on either end of the feed port as shown in Fig. 4a. Full wave simulations in CST for this complete dipole driven by a 50 Ohm discrete port provide the reference results. The plane wave coupling to the dipole is not calculated directly. Instead, the far-field pattern of the dipole is obtained, which can be used later to calculate the dipole response to the plane wave by reciprocity [11, 12]. Therefore, the objective of the segmentation is to divide this dipole into two segments (Fig. 4b-c) and devise a method to reconstruct the far-field produced by the original structure by simulating the two segments separately and combining their far-field contributions.

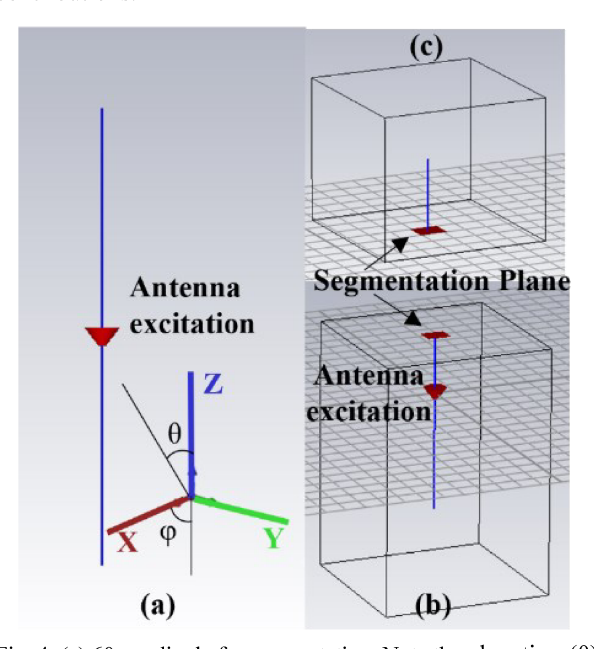


Fig. 4. (a) 60 cm dipole for segmentation. Note the elevation (θ) and azimuth (ϕ) angle definitions in the inset. The dipole is cut asymmetrically, i.e. segment 1 (b) includes roughly three quarters of the dipole length. (c) Segment 2 of the dipole. The wire in this segment is 15.1 cm long.

The cross-section of the dipole in the segmentation plane represents a metal circle surrounded by free space, which does not allow the definition of a discrete port (this requires a connection between two good conductors). However, CST allows for the definition of a waveguide port with an open boundary (red squares in Fig. 4). During the port modal analysis, the open boundary is replaced by perfect magnetic conductor (PMC) boundary condition. However, the field structure of the fundamental mode (which is classified as a TM mode) of the segmentation port resembles that of the dipole mode, Fig. 5. Despite Fig. 5a formally being a TM mode, in the vicinity of the conductor the structure of the mode is very close to the TEM mode in the sense that both the E- and H-field vectors are tangential to the port plane. The TM mode however, has a non-zero cutoff frequency, which eventually determines the size of the waveguide port - a larger port allows the simulation to be performed down to lower frequencies.

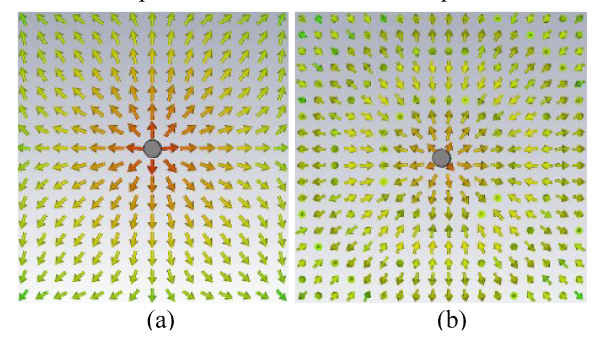


Fig. 5. Electrical field of (a) the segmentation port mode and (b) the dipole mode.

The modes in Fig. 5 are clearly not identical, but close enough such that segmentation is possible, as will be shown below.

Each of the segments is simulated separately in CST, which produces the S-parameter matrices for the segments (a 2x2 matrix for segment 1 and a 1x1 matrix (reflection coefficient) for segment 2), as well as the far-field patterns. The segments are then combined using CST Design Studio (a circuit simulator) as shown in Fig. 6, which produces both the reflection coefficient of the combined model as well as the combined far-field pattern.

The impedance of the combined structure in comparison to the impedance of the original reference dipole is shown in Fig. 7. As can be seen, the dipole impedance is reproduced with an accuracy sufficient for most EMC applications.

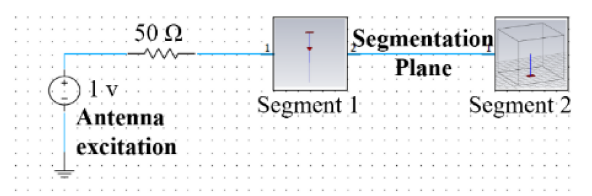


Fig. 6. Cascaded circuit in CST Design Studio used for calculating the field results for each block from the excitations in the network.

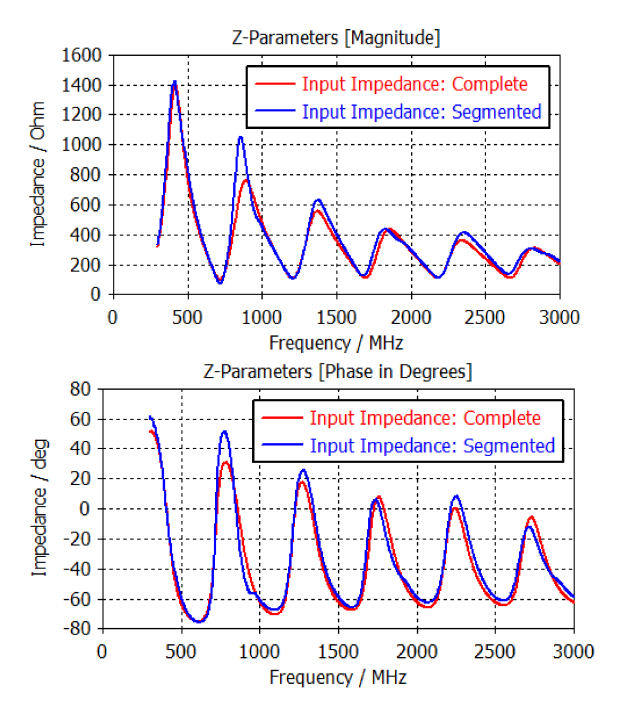
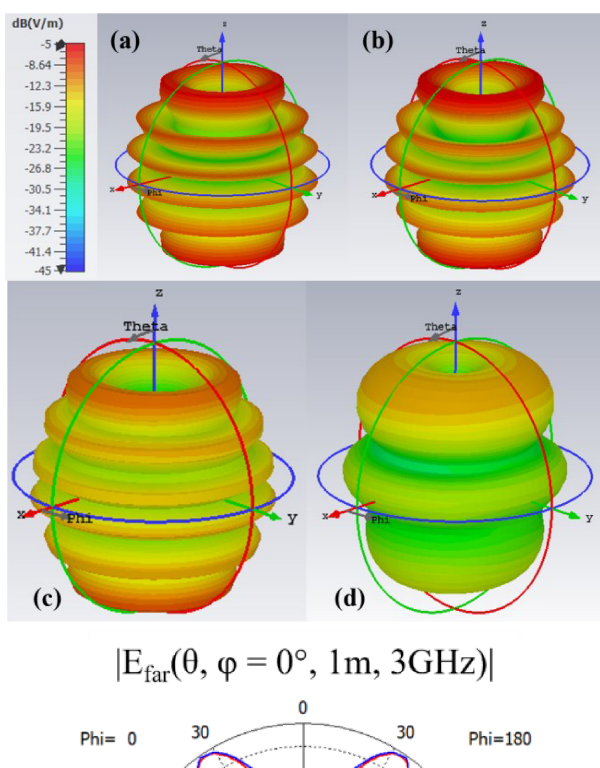


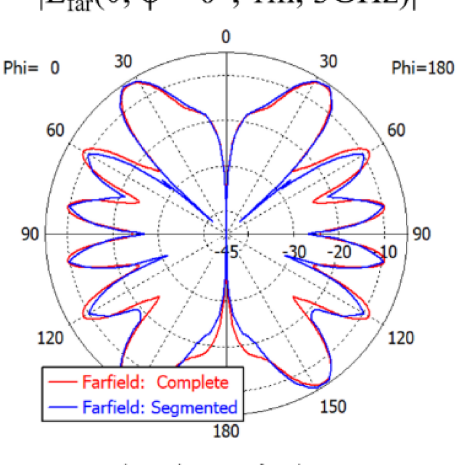
Fig. 7. Magnitude and phase comparisons of the input impedance between the complete and segmented dipole models demonstrate that the quality of segmentation is acceptable.

The far-field for each segment is calculated as a function of the elevation (θ) and azimuth (φ) angles at a fixed reference distance (1 m) and fixed frequency (3 GHz): $E(\theta, \varphi)$. See the inset of Fig. 4a for the definitions of the elevation and azimuth angles relative to the cartesian coordinate system. The fields of each segment are calculated once during the full-wave EM analysis. During the circuit simulation in Fig. 6, the far-fields are scaled according to the defined excitation and combined such that the total field is produced:

$$E_{tot}(\theta, \varphi) = E_{seg1}(\theta, \varphi) + E_{seg2}(\theta, \varphi), \tag{1}$$

Fig. 8 compares the combined far-field pattern with the reference in both 3D and 2D representations and shows the contributions from each segment. As can be seen from the 2D cross-section, the peaks of the combined pattern differ from the reference by no more than 1.3 dB.





 $dBV/m \text{ vs. } \theta \text{ [deg]}$

Fig. 8. Electric far-fields for the straight dipole at 3 GHz, measured 1 m from the origin: (a) reference complete response; (b) total segmented response calculated by summing the contributions from both segments; (c) field contribution from segment 1; (d) field contribution from segment 2; (e) total segmented response plotted against the reference in the θ plane.

III. ANALYSIS OF 2-BLOCK PCB HARNESS COMBINATION

A. 2-Block Electronic Device Model

Having validated the segmentation methodology for the common mode on a straight dipole, the next objective is to apply the methodology to more complicated and realistic structures that exhibit both common and differential mode coupling. Shown in Fig. 9a is a two-block structure consisting of a wire harness and a printed circuit board (PCB). The first segment is a simplified PCB, with the return plane modeled as

a metal plate of 9 x 7 cm (Fig. 9b). It has a short 2 cm trace used to interconnect between the harness signal header pin and any traces routed on the board, which could be characterized in other simulations as in [12]. The trace is 3 mm wide and is elevated 2 mm above the return plane, with a characteristic impedance of 113 Ohms. The connecting structure between the trace and harness consists of two header pins with a wire radius of 0.5 mm, separated by 4 mm. The ground pin is 1 cm in height and connects the ground wire of the harness to the return plane. The harness is a transmission line formed by two parallel wires 2 mm apart, also with a wire radius of 0.5 mm. Fig. 9c shows the 7 cm harness, which forms the second segment.

This structure has significant inherent asymmetries, and thus significant conversion between the common and differential modes at the connector/harness interface should be expected. This structure requires a multi-modal waveguide port definition so that both the common and differential modes can propagate between the blocks. If the structure was segmented using discrete ports only, the common mode would be omitted, resulting in incorrect cascaded S-parameters and far-fields. To correct this, the waveguide port at the interface is defined with two modes: the TEM differential mode and the TM common mode shown in Fig. 10. Notice the similarity between the CM distribution in Fig. 10b and the antenna mode in Fig. 3.

Because of the two modes at the segmentation interface, both segments are now represented by 3x3 S-parameter matrices (Fig. 9d). Ports 2(1) and 2(2) of the PCB segment are the waveguide port modes, which correspond to the modes of the harness waveguide port (denoted as ports 1(1) and 1(2)).

In the Design Studio schematic, the DM and CM connections between the segments are organized to allow the modes to propagate as shown in Fig. 9d. As before, for each block the solver will generate the far-field responses that result from excitations simulated inside the cascaded circuit network. These responses are discussed in the next section. Fig. 9a shows the complete model, which is used as a reference.

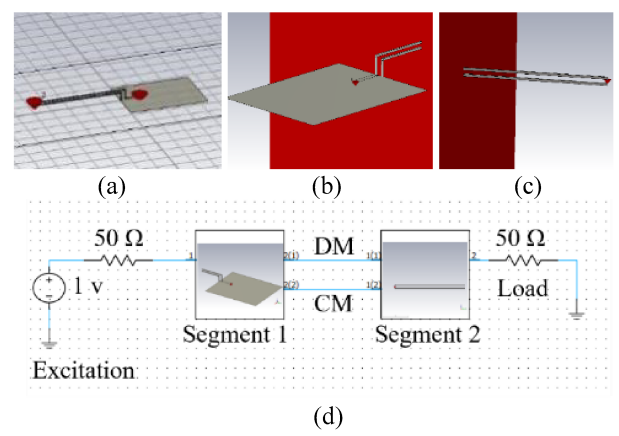


Fig. 9. (a) Complete model for the PCB and harness. This is the reference simulation without any segmentation. (b) PCB block, which is segment 1 in the schematic. (c) Harness block, which is segment 2 in the schematic. (d) Segmented equivalent circuit created using CST's schematic solver. This circuit connects segments 1 and 2 and generates combined results for each block.

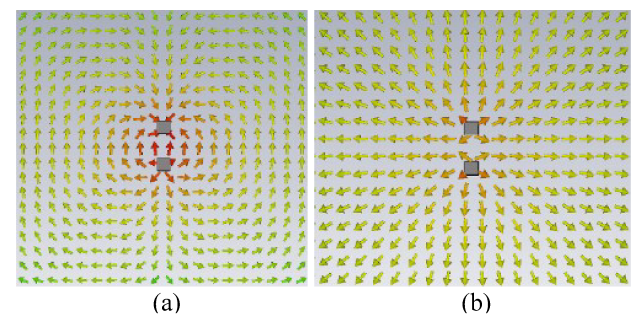


Fig. 10. (a) Differential mode of the waveguide port. (b) Common mode of the waveguide port. This multi-modal port definition is needed to properly propagate currents at the location where the segments are cut.

B. Far-Field Response Calculation

As was done with the straight dipole, CST Design Studio was used to generate the far-field response for the segmented two-block PCB/harness structure. However, this time far-field probes were used to collect the far-field data. This is an alternative way to calculate the far field relative to the far-field monitor used in the previous section. Far-field probes allow for obtaining frequency-dependent far-field data, as opposed to the results at discrete frequencies from far-field monitors, which can suit certain problems better. A larger waveguide port was used in Fig. 9 than in Fig. 4 to lower the cutoff frequency of the port from 1 GHz to 0.3 GHz. Additionally, a relatively small port was used in Fig. 4 so that the port does not act as a "mirror," which distorts the far field monitor results. This is a behavior of CST that does not occur when using far field probes to calculate the far field, hence a large port can be used with far field probes. In this study, probes were placed every 20° in elevation and every 30° degrees in azimuth, as shown in Fig. 11. This results in 130 probes. More probes can be defined if a better angular resolution is required. After the cascaded circuit shown in Fig. 9 is solved, the resulting far-field contributions from each block are summed as in (1) to give the final far-field pattern for the cascaded two-block model.

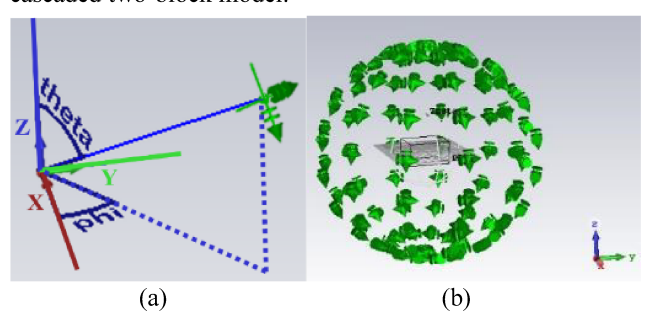


Fig. 11. (a) Angle definitions relative to cartesian coordinate system. (b) Probe definitions for the PCB and harness models. Probes are placed every 20° in elevation and every 30° degrees in azimuth. Thus, 130 probe locations are used to estimate the far-field pattern for each of the models.

Fig. 12 compares the combined total far-field probe response with the reference and shows the contributions from each segment at the two indicated distinct angle combinations. As can be seen, the combined total pattern differs from the

reference by no more than 6 dB and generally by less than 2 dB across much of the frequency range.

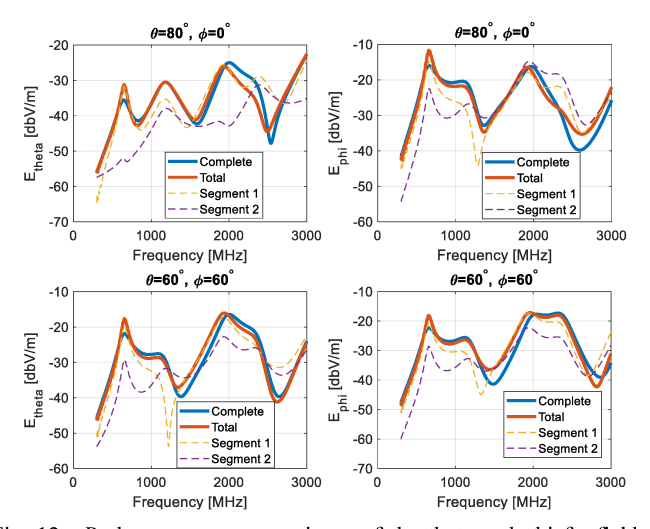


Fig. 12. Probe response comparisons of the theta and phi far-field components for the PCB and harness models. The reference response ("Complete") is shown in blue, the combined segmented response ("Total") in purple, the contribution from segment 1 in red, and the contribution from segment 2 in yellow.

To demonstrate the significance of both the CM and DM modes for the far field calculation, two additional simulations were performed. In each of them, one of the mode connections was disabled, such that energy transfer between the segments could happen through one mode only (Fig. 13).

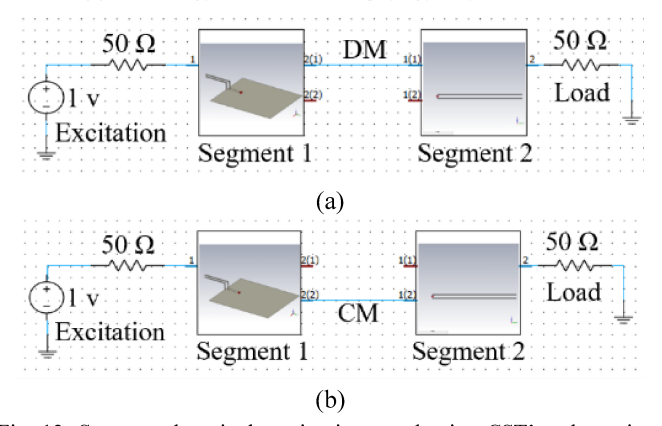


Fig. 13. Segmented equivalent circuit created using CST's schematic solver to generate combined results from each block when: (a) only the differential component is considered (the CM path is disconnected), (b) only the common mode component is considered (the DM path is disconnected).

Fig. 14 compares the contributions from each mode on the probe response at an angle of θ =80°, φ =0°. The far-field response when considering only the CM or DM modes are compared to the reference complete model, as well as when both modes are properly considered to give the total response of the segmented model. As can be seen, the errors when considering only one mode can often be more than 10 dB,

reinforcing the importance of properly accounting from the farfield contributions from both modes.

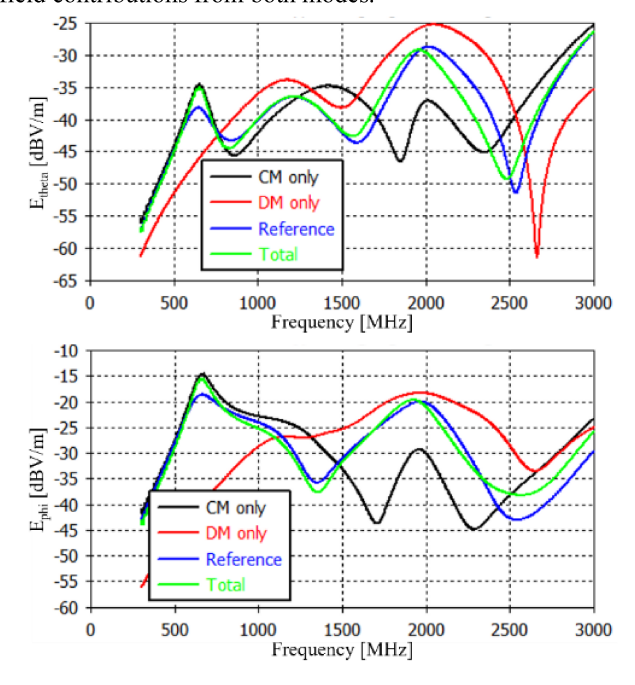


Fig. 14. Contributions from each mode on the probe responses for the theta and phi components at an angle of θ =80°, φ =0°. Shown are the probe responses when only considering the CM mode, when only considering the DM mode, when considering both modes to generate the "Total" response, and the reference "Complete" response.

IV. CONCLUSIONS

A methodology to segment structures with a common (antenna) mode was developed. By introducing a waveguide port at the interface between the segments and defining two propagating modes (CM and DM), it is possible to correctly combine the segments, which are simulated separately, and calculate the S-parameters of the complete structure, as well as the far-field emissions of the device. The far-field pattern and reciprocity theory can later be used to calculate the signals induced in the structure due to external plane wave radiation.

The location of the segmentation interface must be selected carefully. The interface cannot be placed at a "discontinuity," such as where two wires meet at a corner, because the field that exists at this location will not be fully represented by a combination of the propagating port modes. Segmentation is most successful when placing the ports at a location where the model is translationally invariant, preferably at a relatively large distance from discontinuities which cause field disruptions. This is so that the field distribution at the interface can be represented using as few modes as possible.

The methodology was validated first on a dipole, which required defining only the common mode, and then on a more realistic structure containing a PCB with a trace and a two-wire harness. In both cases, the far-field patterns of the segmented models agreed quite well with the total patterns produced by the unsegmented reference structures.

In addition to the total far-fields, the methodology can be used to calculate the contributions of the segments to the far-

field, which is nearly impossible to determine by other methods. This information can be used to determine the most susceptible element of the structure or the one that contributes the most to electromagnetic emissions.

ACKNOWLEDGMENTS

This material is supported by the Office of Naval Research under Grant No. N00014-17-1-3016 and in part by the National Science Foundation under Grant No. IIP-1916535.

REFERENCES

- H. Streitwolf, R. Heinrich, H. Behnke, L. Dallwitz and U. Karsten, "Comparison of radiated immunity tests in different EMC test facilities," 2007 18th International Zurich Symposium on Electromagnetic Compatibility, 2007, pp. 229-232.
- [2] A. -M. Silaghi and A. D. Sabata, "Analysis of Radiated Immunity of an Automotive Display by Means of Testing and Simulation," 2020 43rd International Conference on Telecommunications and Signal Processing (TSP), 2020, pp. 73-76.
- [3] V. S. Reddy, P. Kralicek and J. Hansen, "A Novel Segmentation Approach for Modeling of Radiated Emission and Immunity Test Setups," in *IEEE Transactions on Electromagnetic Compatibility*, vol. 59, no. 6, pp. 1781-1790, Dec. 2017.
- [4] T. Okoshi, Y. Uehara and T. Takeuchi, "The Segmentation Method An Approach to the Analysis of Microwave Planar Circuits (Short Papers)," in *IEEE Transactions on Microwave Theory and Techniques*, vol. 24, no. 10, pp. 662-668, Oct. 1976.
- [5] Shih-Ping Liu and Ching-Kuang C. Tzuang, "Full-wave segmentation analysis of arbitrarily shaped planar circuit," in *IEEE Transactions on Microwave Theory and Techniques*, vol. 45, no. 9, pp. 1554-1562, Sept. 1997.
- [6] J. Hunter, Y. Liu, D. Floyd, A. Hassan, V. Khilkevich, D. Beetner, "Characterization of the Electromagnetic Coupling to UAVs," Annual Directed Energy Science and Technology Symposium, March 2018.
- [7] J. Hunter, S. Xia, A. Harmon, A. Hassan, V. Khilkevich, D. Beetner, "Modeling and Statistical Characterization of Electromagnetic Coupling to Electronic Devices," 2021 United States National Committee of URSI National Radio Science Meeting (USNC-URSI NRSM), 2021, pp. 14-15.
- [8] D. E. Bockelman and W. R. Eisenstadt, "Combined differential and common-mode scattering parameters: theory and simulation," in *IEEE Transactions on Microwave Theory and Techniques*, vol. 43, no. 7, pp. 1530-1539, July 1995.
- [9] Haiyin Wang, Ke-Li Wu and J. Litva, "The higher order modal characteristics of circular-rectangular coaxial waveguides," in *IEEE Transactions on Microwave Theory and Techniques*, vol. 45, no. 3, pp. 414-419, March 1997.
- [10] S. Ahmed and Li Er Ping, "Application of singular value decomposition on FDTD simulation result - a novel approach for modal analysis of complex electromagnetic problems," in *IEEE Microwave and Wireless Components Letters*, vol. 14, no. 11, pp. 519-521, Nov. 2004.
- [11] A. D. Wunsch, "The Receiving Antenna: A Classroom Presentation," in IEEE Antennas and Propagation Magazine, vol. 53, no. 4, pp. 179-187, Aug. 2011.
- [12] S. Xia, J. Hunter, A. Harmon, V. Khilkevich and D. Beetner, "A Fast Cascading Method for Predicting the Coupling from External Plane Waves to PCBs," submitted to 2022 IEEE International Symposium on Electromagnetic Compatibility, Signal & Power Integrity (EMCSI), 2022.